Neutrino-induced pion production from nuclei at medium energies

C. Praet,[*] O. Lalakulich,[†] N. Jachowicz, and J. Ryckebusch

Department of Subatomic and Radiation Physics,

Ghent University,

Proeftuinstraat 86,

B-9000 Gent, Belgium.

(Dated: April 17, 2008)

Abstract

We present a fully relativistic formalism for describing neutrino-induced Δ-mediated single-pion production from nuclei. We assess the ambiguities stemming from the Δ interactions. Variations in the cross sections of over 10% are observed, depending on whether or not magnetic-dipole dominance is assumed to extract the vector form factors. These uncertainties have a direct impact on the accuracy with which the axial-vector form factors can be extracted. Different predictions for $C_5^A(Q^2)$ induce up to 40-50% effects on the Δ-production cross sections. To describe the nucleus, we turn to a relativistic plane-wave impulse approximation (RPWIA) using realistic bound-state wave functions derived in the Hartree approximation to the σ-ω Walecka model. For neutrino energies larger than 1 GeV, we show that a relativistic Fermi-gas model with appropriate binding-energy correction produces comparable results as the RPWIA which naturally includes Fermi motion, nuclear-binding effects and the Pauli exclusion principle. Including Δ medium modifications yields a 20 to 25% reduction of the RPWIA cross section. The model presented in this work can be naturally extended to include the effect of final-state interactions in a relativistic and quantum-mechanical way. Guided by recent neutrino-oscillation experiments, such as MiniBooNE and K2K, and future efforts like MINERνA, we present Q^2, W, and various semi-inclusive distributions, both for a free nucleon and carbon, oxygen and iron targets.

PACS numbers: 13.15.+g, 21.60.-n, 24.10.Jv, 25.30.Pt

─────────────

[*]Electronic address: christophe.praet@ugent.be

[†]Present address: Institut für Theoretische Physik, Universität Giessen, Germany.

1

I. INTRODUCTION

In the last few years, precision measurements of the neutrino-oscillation parameters have driven the interest in medium-energy neutrino physics. The MiniBooNE [1] and K2K [2] collaborations have recently collected a wealth of neutrino data in the 1-GeV energy range [3], where the vast part of the strength can be attributed to quasi-elastic (QE) processes and Δ-mediated one-pion production. A thorough understanding of these cross sections is essential to reduce the systematic uncertainties. In turn, the high-statistics data from these and future neutrino experiments like MINERνA [4] and SciBooNE [5] offer the opportunity to address a variety of topics related to hadronic and nuclear weak physics.

Various theoretical models have been developed to study one-pion production on a free nucleon [6, 7, 8, 9, 10]. These efforts chiefly focus on studying the vector and axial-vector form factors that are introduced to parameterize the incomplete knowledge of the Δ-production vertex. Whereas the vector form factors can be reasonably well determined from electro-production data [7, 9], the axial-vector ones remain troublesome due to the large error flags present in early bubble-chamber neutrino data and sizeable model dependencies in their analyses [10, 11]. Besides, different theoretical calculations of the most important axial form factor, $C_5^A(Q^2)$, reveal highly divergent pictures [12, 13, 14]. Consequently, the Q^2 evolution of the axial form factors and the axial one-pion mass M_A are rather poorly known. Concerning the Δ-decay vertex, it has been established that the traditionally-used decay couplings are not fully consistent with the Rarita-Schwinger field-theoretic description of the Δ particle [15]. Instead, a consistent interaction can be constructed, which couples solely to the physical spin-3/2 part of the Δ propagator [15]. Since planned neutrino-scattering experiments aim at putting further constraints on M_A and the axial form factors, it is important to assess the ambiguities related to the incomplete knowledge of the Δ interactions.

Modeling is made even more challenging by the fact that nuclei are employed as detectors. Thus, various nuclear effects need to be addressed in order to make realistic cross-section predictions. Traditionally, the Fermi motion of the nucleons inside the nucleus is described within the relativistic Fermi gas (RFG) [16, 17]. Owing to its relative simplicity, the RFG model has been the preferred nuclear model in neutrino-event generators. Going beyond the RFG, realistic bound-state wave functions can be calculated within a relativistic shell model [17, 18], or by adopting spectral-function approaches that extend beyond the mean-field pic-

ture [19, 20, 21, 22]. A comparison of these models provides insight into the nuclear-model dependence of the computed cross sections. Another nuclear effect stems from the fact that the Δ properties are modified in a medium [23], generally resulting in a shift of the peak position and a collisional broadening of the width. Finally, one must consider the final-state interactions (FSI) of the outgoing pion and nucleon. To study the effect of FSI, recent efforts have resorted to a combination of semi-classical and Monte-Carlo techniques [24, 25]. Based on these results, it is clear that FSI mechanisms produce by far the largest nuclear effect on one-pion production computations.

In this work, we present a fully relativistic formalism that can serve as a starting point to investigate Δ-mediated one-pion production from nuclei. Recognizing the ability of the new generation of experiments to measure both inclusive and semi-inclusive observables, we develop a framework that is geared towards a detailed study of various distributions, like Q^2, W, energy and scattering-angle dependences. To model nuclear effects, we turn to the relativistic plane-wave impulse approximation, using relativistic bound-state wave functions that are calculated in the Hartree approximation to the σ-ω Walecka model [26]. This approach was successfully applied in QE nucleon-knockout studies [18, 27, 28, 29], and includes the effects of Fermi motion, nuclear binding and the Pauli exclusion principle in a natural way. Medium modifications of the Δ particle are taken into account along the lines of Ref. [23]. We investigate the sensitivity of the cross section to uncertainties in the Δ couplings. Then, we proceed with the nuclear-model dependence of our results, by comparing with RFG calculations. Our findings in this regard are of great importance to neutrino experiments that employ the RFG model in the event generators. The formalism outlined in this work is an ideal starting ground to implement also FSI effects in a fully relativistic and quantum-mechanical way. The discussion of FSI mechanisms, however, falls beyond the scope of the present paper.

The paper is organized as follows. Section II introduces the formalism for the elementary Δ-mediated one-pion production process. The third section deals with the nuclear model and discusses the framework for the description of neutrino-nucleus interactions. Numerical results are presented in section IV. In section V, we summarize our conclusions.

II. CHARGED-CURRENT PION NEUTRINOPRODUCTION ON THE NUCLEON

A. Cross section

For a free proton target, the charged-current (CC) process under study is

$$\nu_\mu + p \xrightarrow{\Delta^{++}} \mu^- + p + \pi^+. \tag{1}$$

The corresponding reactions for a free neutron are

$$\nu_\mu + n \xrightarrow{\Delta^+} \mu^- + p + \pi^0,$$
$$\nu_\mu + n \xrightarrow{\Delta^+} \mu^- + n + \pi^+. \tag{2}$$

Isospin considerations allow one to relate the strength of the above reactions

$$\sigma(W^+ p \xrightarrow{\Delta^{++}} p\pi^+) = 9\sigma(W^+ n \xrightarrow{\Delta^+} n\pi^+)$$
$$= \frac{9}{2}\sigma(W^+ n \xrightarrow{\Delta^+} p\pi^0), \tag{3}$$

where W^+ denotes the exchanged weak vector boson. In a laboratory frame of reference, the corresponding differential cross section is given by [30]

$$d^9\sigma = \frac{1}{\beta} \frac{m_\nu}{E_\nu} \frac{m_l}{E_l} \frac{d^3\vec{k}_l}{(2\pi)^3} \frac{m_N}{E_N} \frac{d^3\vec{k}_N}{(2\pi)^3} \frac{d^3\vec{k}_\pi}{2E_\pi(2\pi)^3}$$
$$\times \overline{\sum}_{fi} |M_{fi}^{(free)}|^2 (2\pi)^4 \delta^{(4)}(k_\nu + k_{N,i} - k_l - k_\pi - k_N). \tag{4}$$

Figure 1 defines our conventions for the kinematical variables. The target nucleon has four-momentum $k_{N,i} = (m_N, \vec{0})$, with m_N the nucleon's mass. We write $k_\nu = (E_\nu, \vec{k}_\nu)$ for the incoming neutrino, $k_l = (E_l, \vec{k}_l)$ for the outgoing muon, $k_\pi = (E_\pi, \vec{k}_\pi)$ for the outgoing pion and $k_N = (E_N, \vec{k}_N)$ for the outgoing nucleon. The xyz coordinate system is chosen such that the z axis lies along the momentum transfer $\vec{q}$, the y axis along $\vec{k}_\nu \times \vec{k}_l$, and the x axis in the lepton-scattering plane. In Eq. (4), the incoming neutrino's relative velocity $\beta = |\vec{k}_\nu|/E_\nu$ is 1. The neutrino mass m_ν will cancel with the neutrino normalization factor appearing in the lepton tensor. The δ-function expresses energy-momentum conservation and $\overline{\sum}_{fi} |M_{fi}^{(free)}|^2$ denotes the squared invariant matrix element, appropriately averaged over initial spins and summed over final spins. Using the δ-function to integrate over the outgoing nucleon's three-momentum and the magnitude of the pion's momentum, one arrives at the fivefold cross
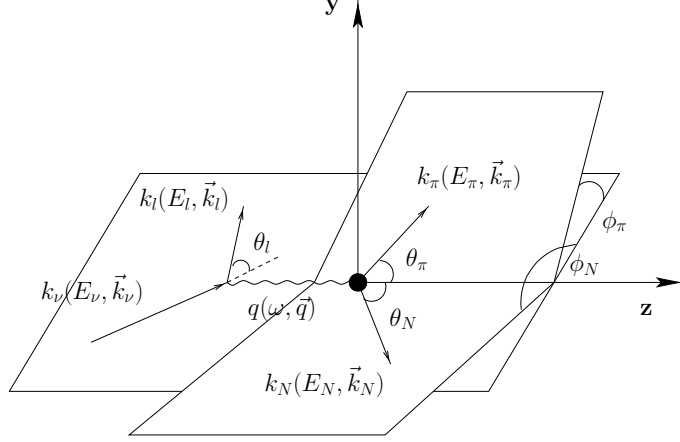
FIG. 1: Kinematics for neutrino-induced charged-current one-pion production on the nucleon.

section

$$\frac{d^5\sigma}{dE_l d\Omega_l d\Omega_\pi} = \frac{m_\nu m_l |\vec{k}_l| m_N |\vec{k}_\pi|}{2(2\pi)^5 E_\nu |E_N + E_\pi (|\vec{k}_\pi|^2 - \vec{q} \cdot \vec{k}_\pi)/|\vec{k}_\pi|^2|} \times \overline{\sum}_{fi} |M_{fi}^{(free)}|^2,$$

(5)

where the solid angles Ω_l and Ω_π define the direction of the outgoing muon and pion respectively.

B. Matrix element for resonant one-pion production

Next to the kinematic phase-space factor, Eq. (5) contains the squared invariant matrix element

$$\overline{\sum}_{fi} |M_{fi}^{(free)}|^2 = \frac{1}{2} \sum_{\substack{s_\nu; s_l \\ s_{N,i}; s_N}} \left[M_{fi}^{(free)} \right]^\dagger M_{fi}^{(free)}.$$

(6)

Here, the sum over final muon and nucleon spins is taken. Averaging over the initial nucleon's spin, $s_{N,i}$, leads to a factor 1/2. An explicit expression for the invariant matrix element is obtained by applying the Feynman rules in momentum space. Writing

$$M_{fi}^{(free)} = i \frac{G_F \cos\theta_c}{\sqrt{2}} < J_{had}^{\rho(free)} > S_{W,\rho\sigma} < J_{lep}^\sigma >,$$

(7)

with G_F the Fermi constant and θ_c the Cabibbo angle, one distinguishes the hadron current

$$< J_{had}^{\rho(free)} >= \overline{u}(k_N, s_N)\Gamma_{\Delta\pi N}^\mu S_{\Delta,\mu\nu}\Gamma_{WN\Delta}^{\nu\rho} u(k_{N,i}, s_{N,i}),$$

(8)

5

the weak boson propagator

$$S_{W,\rho\sigma} = \frac{g_{\rho\sigma} M_W^2}{Q^2 + M_W^2}; \quad Q^2 = -q_\mu q^\mu, \tag{9}$$

and the lepton current

$$< J_{lep}^\sigma > = \overline{u}(k_l, s_l) \gamma^\sigma (1 - \gamma_5) u(k_\nu, s_\nu). \tag{10}$$

Clearly, the least-known physics is contained in the vertex functions of the matrix element of Eq. (8). For the Δ-production vertex, we adopt the form [8]

$$\Gamma_{WN\Delta}^{\nu\rho}(k_\Delta, q) = \left[\frac{C_3^V(Q^2)}{m_N} (g^{\nu\rho} \not{q} - q^\nu \gamma^\rho) + \frac{C_4^V(Q^2)}{m_N^2} (g^{\nu\rho} q \cdot k_\Delta - q^\nu k_\Delta^\rho) + \frac{C_5^V(Q^2)}{m_N^2} (g^{\nu\rho} q \cdot k_{N,i} - q^\nu k_{N,i}^\rho) + g^{\nu\rho} \right.$$
$$\left. + \frac{C_3^A(Q^2)}{m_N} (g^{\nu\rho} \not{q} - q^\nu \gamma^\rho) + \frac{C_4^A(Q^2)}{m_N^2} (g^{\nu\rho} q \cdot k_\Delta - q^\nu k_\Delta^\rho) + C_5^A(Q^2) g^{\nu\rho} + \frac{C_6^A(Q^2)}{m_N^2} q^\nu q^\rho, \right. \tag{11}$$

where a set of vector (C_i^V, $i = 3..6$) and axial (C_i^A, $i = 3..6$) form factors are introduced. These form factors are constrained by physical principles and experimental data. Imposing the conserved vector current (CVC) hypothesis leads to $C_6^V = 0$. The partially-conserved axial current (PCAC) hypothesis, together with the pion-pole dominance assumption, yields the following relation between C_5^A and the pseudoscalar form factor C_6^A

$$C_6^A = C_5^A \frac{m_N^2}{Q^2 + m_\pi^2}. \tag{12}$$

At $Q^2 = 0$, the off-diagonal Goldberger-Treiman relation gives $C_5^A = 1.2$ [9]. Furthermore, CVC entails that the weak vector current and the isovector part of the electromagnetic current are components of the same isospin current. Consequently, after extracting the electromagnetic form factors from electroproduction data, the $C_i^V, i = 3, 4, 5$ follow immediately by applying the appropriate transformations in isospin space. To extract the vector form factors, it has been established that the magnetic-dipole (M1) dominance of the electromagnetic $N \to \Delta$ transition amplitude is a reasonable assumption [31]. This M1 dominance leads to the conditions [32]

$$C_4^V = -C_3^V \frac{m_N}{W}, \quad C_5^V = 0, \tag{13}$$

where W is the invariant mass, defined as $W = \sqrt{k_\Delta^2}$. For C_3^V, a modified-dipole parameterization is extracted [8, 24, 32]

$$C_3^V = \frac{1.95 D_V}{1 + Q^2/4M_V^2}, \tag{14}$$

6

with $D_V = (1 + Q^2/M_V^2)^{-2}$ the dipole function and $M_V = 0.84$ GeV. In Eq. (14), the faster-than-dipole fall-off reflects the fact that the Δ is a more extended object than a nucleon. Within this scheme, it is possible to relate all weak vector form factors to C_3^V. More recently, a direct analysis of the electroproduction helicity amplitudes from JLab and Mainz experiments resulted in an alternative parameterization of the weak vector form factors [9]

$$C_3^V = \frac{2.13 D_V}{1 + Q^2/4M_V^2}, \quad C_4^V = \frac{-1.51}{2.13} C_3^V,$$
$$C_5^V = \frac{0.48 D_V}{1 + Q^2/0.776 M_V^2}, \tag{15}$$

attributing a non-zero strength to the weak vector form factor C_5^V. The axial form factors are even more difficult to determine, in the sense that they are only constrained by the bubble-chamber neutrino data. A widely used parameterization is given by [8, 24, 32]

$$C_5^A = \frac{1.2}{(1 + Q^2/M_A^2)^2} \frac{1}{1 + Q^2/3M_A^2},$$
$$C_4^A = -\frac{C_5^A}{4}, \quad C_3^A = 0, \tag{16}$$

where $M_A = 1.05$ GeV. However, there still resides a great deal of uncertainty in the axial form factors or, equivalently, in C_5^A. The extracted axial-mass value, for example, is heavily model-dependent [10, 11]. A re-analysis [10] of ANL data within a model that includes background contributions next to the Δ-pole mechanism reveals a $C_5^A(0)$ value that is lower than the one predicted by the Goldberger-Treiman relation. This result is corroborated by some recent form-factor calculations, within a chiral constituent-quark (χCQ) model [12] and lattice QCD framework [13, 14]. Figure 2 compares both theoretical calculations with the phenomenological fit of Eq. (16). It can be clearly seen that all three approaches exhibit highly divergent Q^2 evolutions.

The Rarita-Schwinger spin-3/2 propagator for the Δ reads

$$S_{\Delta,\mu\nu}(k_\Delta) = \frac{\slashed{k}_\Delta + M_\Delta}{k_\Delta^2 - M_\Delta^2 + iM_\Delta\Gamma}\left(g_{\mu\nu} - \frac{\gamma_\mu\gamma_\nu}{3} - \frac{2k_{\Delta,\mu}k_{\Delta,\nu}}{3M_\Delta^2} - \frac{\gamma_\mu k_{\Delta,\nu} - \gamma_\nu k_{\Delta,\mu}}{3M_\Delta}\right), \tag{17}$$

where $M_\Delta = 1.232$ GeV and Γ stands for the free decay width.

A common way of describing the Δ decay is through the interaction Lagrangian

$$\mathcal{L}_{\pi N\Delta} = \frac{f_{\pi N\Delta}}{m_\pi}\overline{\psi}_\mu \vec{T}^\dagger (\partial^\mu \vec{\phi})\psi + h.c, \tag{18}$$
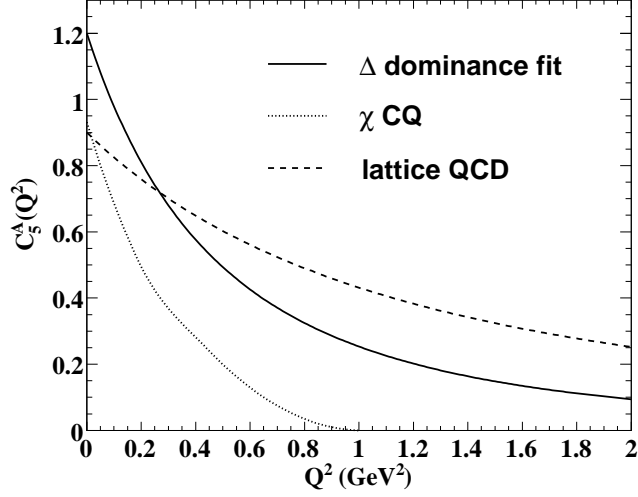
7

FIG. 2: Different results for the axial transition form factor $C_5^A(Q^2)$. The full line represents a phenomenological fit to ANL and BNL data within a Δ-dominance model (Eq. 16). The dashed line shows a quenched lattice result, and is parameterized as $C_5^A(Q^2) = C_5^A(0)(1 + Q^2/\tilde{M}_A^2)^{-2}$, $C_5^A(0) = 0.9$ and $\tilde{M}_A = 1.5$ GeV [14]. The dotted line corresponds to a χCQ result, and is taken from Ref. [12].

where ψ_μ, $\vec{\phi}$ and ψ denote the spin-3/2 Rarita-Schwinger field, the pion field and the nucleon field respectively. The operator $\vec{T}$ is the isospin $1/2 \to 3/2$ transition operator. From (18), one derives the simple vertex function

$$\Gamma^\mu_{\Delta\pi N}(k_\pi) = \frac{f_{\pi N\Delta}}{m_\pi} k_\pi^\mu, \tag{19}$$

and the corresponding energy-dependent width

$$\Gamma(W) = \frac{1}{12\pi} \frac{f_{\pi N\Delta}^2}{m_\pi^2 W} |\vec{q}_{cm}|^3 (m_N + E_N), \tag{20}$$

with

$$|\vec{q}_{cm}| = \frac{\sqrt{(W^2 - m_\pi^2 - m_N^2)^2 - 4m_\pi^2 m_N^2}}{2W}. \tag{21}$$

Requiring that $\Gamma(M_\Delta)$ equals the experimentally determined value of 120 MeV, one obtains $f_{\pi N\Delta} = 2.21$. An alternative choice for the $\Delta\pi N$ interaction Lagrangian is provided by

$$\mathcal{L}_{\pi N\Delta} = \frac{f_{\pi N\Delta}^*}{m_\pi M_\Delta} \epsilon^{\alpha\beta\mu\nu} \overline{G}_{\beta\alpha} \gamma_\mu \gamma_5 \vec{T}^\dagger (\partial_\nu \vec{\phi}) \psi, \tag{22}$$

where $G_{\beta\alpha} = \partial_\beta \psi_\alpha - \partial_\alpha \psi_\beta$. This form has been proposed by Pascalutsa et al. [15], who point out that many of the traditional couplings, like the one in Eq. (18), give rise to unwanted

spin-1/2 contributions to the cross section. The interaction of Eq. (22), however, couples only to the physical, spin-3/2 part of the Δ propagator. With the interaction Lagrangian of Eq. (22) the vertex function becomes

$$\Gamma^\mu_{\Delta\pi N}(k_\pi, k_\Delta) = \frac{f^*_{\pi N\Delta}}{m_\pi M_\Delta}\epsilon^{\mu\alpha\beta\gamma}k_{\pi,\alpha}\gamma_\beta\gamma_5 k_{\Delta,\gamma}. \tag{23}$$

Calculating the decay width from Eq. (23) leads to the same expression as in Eq. (20), implying $f^*_{\pi N\Delta} = f_{\pi N\Delta} = 2.21$.

Combining formulas (6) to (10), the squared invariant matrix element can be cast in the form

$$\overline{\sum}_{fi}|M^{(free)}_{fi}|^2 = \frac{G_F^2\cos^2\theta_c M_W^4}{2(M_W^2 + Q^2)^2}H^{\rho\sigma}_{(free)}L_{\rho\sigma}, \tag{24}$$

where the leptonic tensor is given by

$$L_{\rho\sigma} = \frac{2}{m_\nu m_l}(k_{\nu,\rho}k_{l,\sigma} + k_{\nu,\sigma}k_{l,\rho} - k_\nu \cdot k_l g_{\rho\sigma} - i\epsilon_{\alpha\rho\beta\sigma}k_\nu^\alpha k_l^\beta), \tag{25}$$

with the definition $\epsilon_{0123} = +1$. Introducing the shorthand notation $\mathcal{O}^\sigma = \Gamma^\mu_{\Delta\pi N}S_{\Delta,\mu\nu}\Gamma^{\nu\sigma}_{WN\Delta}$, one arrives at the following expression for the hadronic tensor

$$H^{\rho\sigma}_{(free)} = \frac{1}{8m_N^2}\text{Tr}\Big((\not k_{N,i} + m_N)\widetilde{\mathcal{O}}^\rho(\not k_N + m_N)\mathcal{O}^\sigma\Big), \tag{26}$$

where $\widetilde{\mathcal{O}}^\rho = \gamma_0(\mathcal{O}^\rho)^\dagger\gamma_0$.

III. CHARGED-CURRENT PION NEUTRINOPRODUCTION FROM A NUCLEUS

Turning to nuclear targets, a schematical representation of the reaction under study is given by

$$\nu_\mu + A \xrightarrow{\Delta} \mu^- + (A - 1) + N + \pi, \tag{27}$$

where A denotes the mass number of the target nucleus. Compared to the free-nucleon case, one now needs to consider the residual nucleus $k_{A-1} = (E_{A-1}, \vec{k}_{A-1})$ as an extra particle in the hadronic final state. Following the same line of reasoning as in section II A, the lab-frame

cross section corresponding to the process of Eq. (27) becomes

$$
\frac{d^8\sigma}{dE_l d\Omega_l dE_\pi d\Omega_\pi d\Omega_N} =
$$
$$
\frac{m_\nu m_l |\vec{k}_l| m_N m_{A-1} |\vec{k}_\pi| |\vec{k}_N|}{2(2\pi)^8 E_\nu |E_{A-1} + E_N + E_N \vec{k}_N \cdot (\vec{k}_\pi - \vec{q})/|\vec{k}_N|^2|}
$$
$$
\times \overline{\sum_{fi}} |M_{fi}^{(bound)}|^2.
$$
(28)

A. Relativistic bound-state wave functions

The invariant matrix element in (28) carries the tag *bound* and involves nuclear many-body currents between initial and final nuclear wave functions. In medium-energy physics, however, one usually resorts to a number of assumptions that allow a reduction of the nuclear-current matrix elements to a form similar to Eq. (8). Here, we summarize the main approximations that enable this simplification and refer to Ref. [33] for the more detailed and analytic considerations. First, we only consider processes where the residual $(A-1)$ system is left with an excitation energy not exceeding a few tens of MeV. The major fraction of the transferred energy is carried by the outgoing pion and nucleon. Further, we adopt the impulse approximation (IA): the nuclear many-body current is replaced by a sum of one-body current operators, exempt from medium effects. Assuming an independent-particle model (IPM) for the initial and final nuclear wave functions, the hadronic current matrix elements can be written in the form of Eq. (8), whereby the initial-nucleon free Dirac spinor is replaced by a bound-state spinor [33]. This approach, where the outgoing nucleon and pion remain unaffected by the nuclear medium, is generally referred to as the relativistic plane-wave impulse approximation (RPWIA).

The single-particle wave functions used in this work are determined in the Hartree approximation to the σ-ω Walecka model, using the $W1$ parameterization for the different field strengths [26]. They are written as

$$
\Psi_{\alpha,m}(\vec{r}) = \begin{pmatrix} i\frac{G(r)}{r} \mathcal{Y}_{+\kappa,m}(\hat{\vec{r}}) \\ -\frac{F(r)}{r} \mathcal{Y}_{-\kappa,m}(\hat{\vec{r}}) \end{pmatrix},
$$
(29)

where m is the magnetic quantum number and α stands for all other quantum numbers that specify a single-particle orbital. In the definition of the spherical two-spinors, a generalized

angular momentum κ is introduced. The momentum wave functions are obtained from

$$\mathcal{U}_{\alpha,m}(\vec{p}) = \frac{1}{(2\pi)^{3/2}} \int \Psi_{\alpha,m}(\vec{r}) e^{-i\vec{p}\cdot\vec{r}} d\vec{r}. \tag{30}$$

The result is

$$\mathcal{U}_{\alpha,m}(\vec{p}) = i^{(1-l)} \sqrt{\frac{2}{\pi}} \frac{1}{p} \begin{pmatrix} g(p)\mathcal{Y}_{+\kappa,m}(\hat{\vec{p}}) \\ -f(p)\mathcal{Y}_{-\kappa,m}(\hat{\vec{p}}) \end{pmatrix}, \tag{31}$$

with

$$g(p) = \int_0^\infty G(r)\hat{j}_l(pr) dr, \tag{32}$$

and

$$f(p) = \mathrm{sgn}(\kappa) \int_0^\infty F(r)\hat{j}_{\bar{l}}(pr) dr, \quad \bar{l} = \begin{pmatrix} l+1, & \kappa < 0 \\ l-1, & \kappa > 0 \end{pmatrix}. \tag{33}$$

In (32) and (33), $\hat{j}_l(x) = x\, j_l(x)$ is the Ricatti-Bessel function.

Returning to the calculation of the squared invariant matrix element in (28), the following factor appears

$$S_\alpha(\vec{p}) = \frac{1}{2j+1} \sum_m \mathcal{U}_{\alpha,m}(\vec{p})\overline{\mathcal{U}}_{\alpha,m}(\vec{p}). \tag{34}$$

This expression, referred to as the bound-state propagator, can be cast in a form which is similar to the free-nucleon projection operator [34]. One finds

$$S_\alpha(\vec{p}) = (\not{k}_\alpha + M_\alpha), \tag{35}$$

with the definitions

$$\begin{aligned} M_\alpha &= \frac{1}{(2\pi)^3} \frac{\pi}{p^2} \left(g^2(p) - f^2(p) \right), \\ E_\alpha &= \frac{1}{(2\pi)^3} \frac{\pi}{p^2} \left(g^2(p) + f^2(p) \right), \\ \vec{k}_\alpha &= \frac{1}{(2\pi)^3} \frac{\pi}{p^2} \left(2g(p)f(p)\hat{\vec{p}} \right). \end{aligned} \tag{36}$$

In other words, the hadronic tensor for scattering off a bound nucleon is readily found from the free-nucleon one in Eq. (26) by making the replacement

$$\frac{1}{2} \frac{(\not{k}_{N,i} + m_N)}{2m_N} \longrightarrow (2\pi)^3 (\not{k}_\alpha + M_\alpha). \tag{37}$$

Figure 3 shows the momentum wave functions of Eqs. (32) and (33) for a proton belonging to a specified carbon shell. Owing to the small contribution of the lower wave-function component, the quantities M_α and E_α are almost equal in strength.
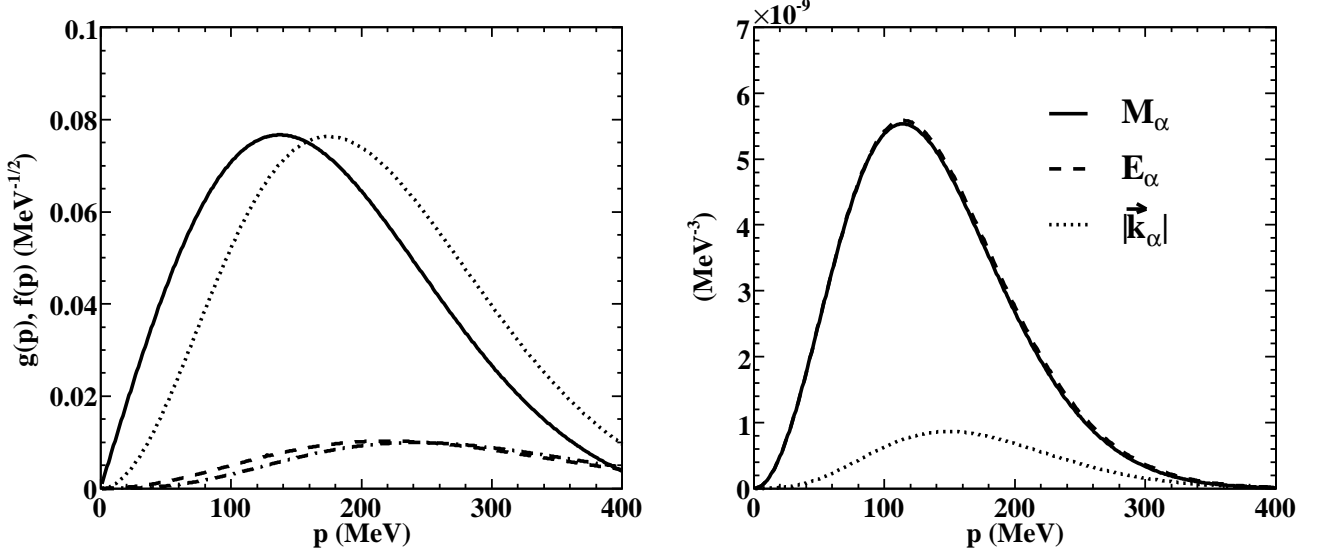
FIG. 3: The left panel shows the momentum wave functions for the carbon nucleus. The full (dashed) line corresponds to $g(p)$ ($f(p)$) for a $1s_{1/2}$ proton, the dotted (dash-dotted) line represents $g(p)$ ($f(p)$) for a $1p_{3/2}$ proton. In the right panel, the quantities defined in Eq. (36) are shown for a $1p_{3/2}$-shell ^{12}C proton.

B. Medium modifications of Δ properties

In a nuclear environment, the Δ mass and width will be modified with respect to its free values. These medium modifications can be estimated by calculating the in-medium Δ self-energy, as was e.g. done in Ref. [23]. The real part of the Δ self-energy causes a shift of the resonance position, whereas the imaginary part is related to the decay width. Medium modifications for the width result from the competition between a Pauli-blocking correction, reducing the free decay width, and a term proportional to the imaginary part of the Δ self-energy, including various meson and baryon interaction mechanisms and, therefore, enhancing the free decay width. A convenient parameterization for the medium-modified mass and width of the Δ is given in Ref. [23], in terms of the nuclear density ρ. For our purposes, we shall adopt an average nuclear density $\rho = 0.75\rho_0$, with ρ_0 the equilibrium density. Then, at the Δ peak, we calculate the following shifts

$$M_\Delta \longrightarrow M_\Delta + 30 \text{ MeV},$$
$$\Gamma \longrightarrow \Gamma + 40 \text{ MeV}. \tag{38}$$

In Ref. [35], a similar recipe was used to accommodate medium modifications in the calculation of $^{12}\text{C}(\gamma, \text{pn})$ and $^{12}\text{C}(\gamma, \text{pp})$ cross sections. There, the computations proved to compare favorably with the data in an energy regime where the reaction is dominated by Δ creation.

IV. RESULTS AND DISCUSSION

In this section, we present computations for the process

$$\nu_\mu + p \xrightarrow{\Delta^{++}} \mu^- + p + \pi^+, \tag{39}$$

the strength of which can be straightforwardly related to the other channels listed in Eq. (2) by applying the isospin relations of Eq. (3). Throughout this work, the cross sections are shown per nucleon, meaning that the RPWIA results are scaled to the number of protons in the target nucleus. Unless otherwise stated, we use the vector form factors derived in the M1-dominance model (Eqs. (13) and (14)), the axial form factors of Eq. (16) with $M_A = 1.05$ GeV, and the *traditional* $\Delta\pi N$ coupling defined in Eq. (18). For the RFG calculations, we adopt $k_F = 225$ MeV and an average binding energy of $E_B = 20$ MeV. The latter value can be considered as a good estimate for the weighted average of the centroids of the single-particle strength distributions in typical even-even nuclei near the closed shells [36].

A. WNΔ and $\Delta\pi$N couplings

Before discussing the nuclear effects described in section III, we address some topics related to the elementary Δ couplings introduced in section II B. Figure 4 appraises the sensitivity of the Q^2 distribution to uncertainties residing in the vector and axial-vector form factors. The left-hand panel contrasts the widely used M1-dominance parameterization for the vector form factors with a more recent fit to electroproduction helicity amplitudes, which extends beyond magnetic-dipole dominance [9]. With the Lalakulich fit of Eq. (15) one finds cross sections which are about 10% higher than those obtained with the M1-dominance form factors of Eqs. (13) and (14). The discrepancy between both parameterizations is significant, as vector form factors are usually regarded as well-known when they are used as input to extract the far less known axial form factors from neutrino-scattering data.
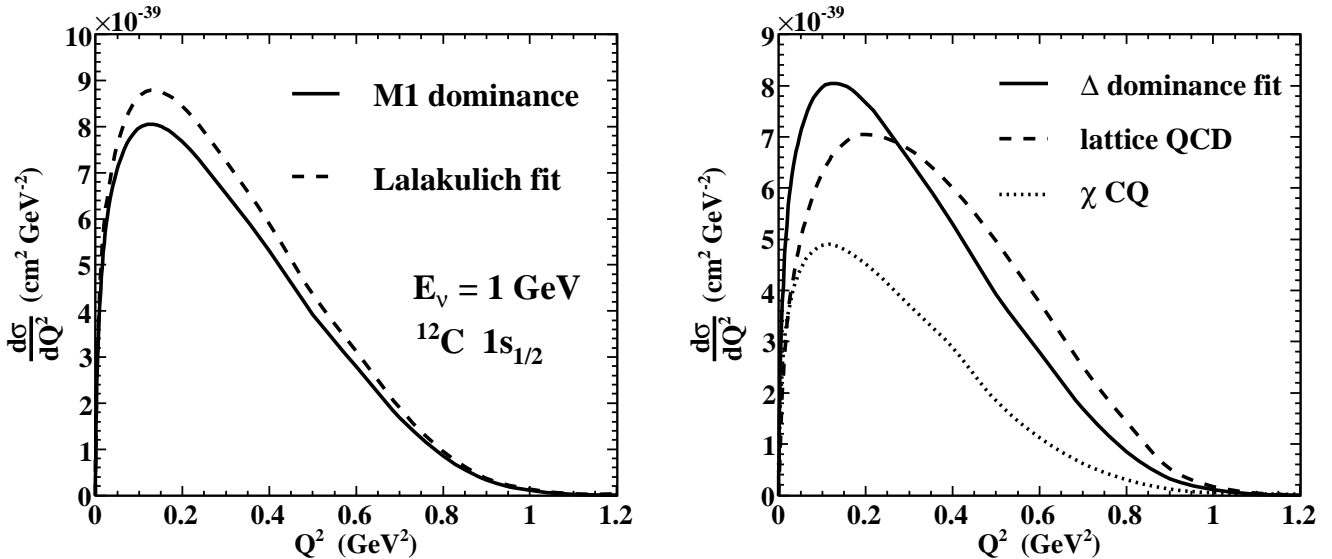
FIG. 4: Q^2 evolution of the Δ^{++}-production cross sections for a $1s_{1/2}$ ^{12}C proton and an incoming neutrino energy of 1 GeV. In the left panel, the full (dashed) line corresponds to the vector form-factor parameterization of Eqs. (13) and (14) (Eq. (15)). The right panel studies the sensitivity of the cross sections to the various parameterizations for $C_5^A(Q^2)$, contained in Fig. 2.

As pointed out in section II B, the current situation for the axial-vector form factors is somewhat more dramatic. To see how uncertainties in $C_5^A(Q^2)$ affect the cross section, we have performed computations with both the phenomenological result of Eq. (16) and the theoretical calculations shown in Fig. 2. The right-hand panel of Fig. 4 shows what this implies for the Q^2 distribution. Clearly, the Q^2 evolution of the Δ-production cross section exhibits a strong sensitivity to the adopted $C_5^A(Q^2)$ parameterization. Near $Q^2 = 0$, cross sections using the χCQ- and QCD-model results are about 40% lower than the calculation with the Δ-dominance fit. This is almost entirely due to the difference in $C_5^A(0)$ values, which yields a ratio of $(0.9)^2/(1.2)^2 \approx 0.56$ for the dominant cross-section contribution. The rapid fall-off predicted by the χCQ model results in cross-section values that are much lower over the whole Q^2 range. On the other hand, the QCD calculation foretells a less steep dipole dependence, leading to more strength towards higher Q^2 values. The χCQ result for C_5^A halves the integrated cross section with respect to the calculation with the Δ-dominance fit. To investigate the impact of different Δ-decay couplings, we have computed W-distributions using both the traditional coupling of Eq. (18) and the Pascalutsa coupling
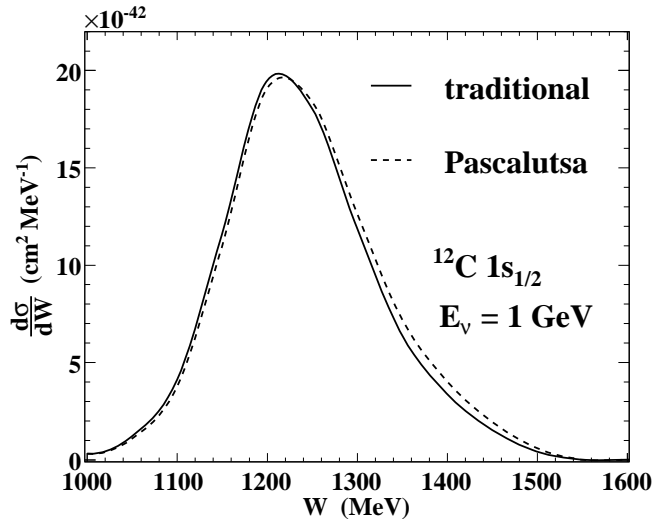
14

FIG. 5: Invariant-mass dependence of the Δ^{++}-production cross sections for a $1s_{1/2}$ ^{12}C proton and an incoming neutrino energy of 1 GeV. The hadronic invariant mass is defined as $W = \sqrt{(k_\pi + k_N)^2}$. The full (dashed) line uses the $\Delta\pi N$ coupling of Eq. (18) (Eq. (22)).

of Eq. (22). The results are shown in Fig. 5, where it can be seen that differences between the two approaches are small. Although the Pascalutsa coupling yields higher values in the tail of the W-distribution, we infer an overall effect that does not exceed the 2% level.

B. Nuclear-model effects

In this subsection, the results of section IV A will be put in a more general perspective. To this end, we will compare neutrino-nucleus with neutrino-nucleon cross sections. Figure 6 shows how the total strength for the process in Eq. (39) varies with the incoming neutrino energy. Under the same kinematical conditions and with similar input for the Δ couplings, our results for the elementary process compare very well with the predictions published in Ref. [10]. Turning to the predictions for target nuclei, Fig. 6 shows how the elementary cross section is halved near threshold. For higher incoming energies, the effect dwindles to 20% at $E_\nu = 800$ MeV and 8% at $E_\nu = 2$ GeV. Most strikingly, the RFG calculations are in good to excellent agreement with both the carbon and iron RPWIA results. The only discernable feature of Fig. 6 is that the iron curve exceeds the carbon and RFG ones by roughly 15% just beyond threshold. This can be understood after recognizing that the iron result is largely due to outer-shell protons, which are less bound than the corresponding
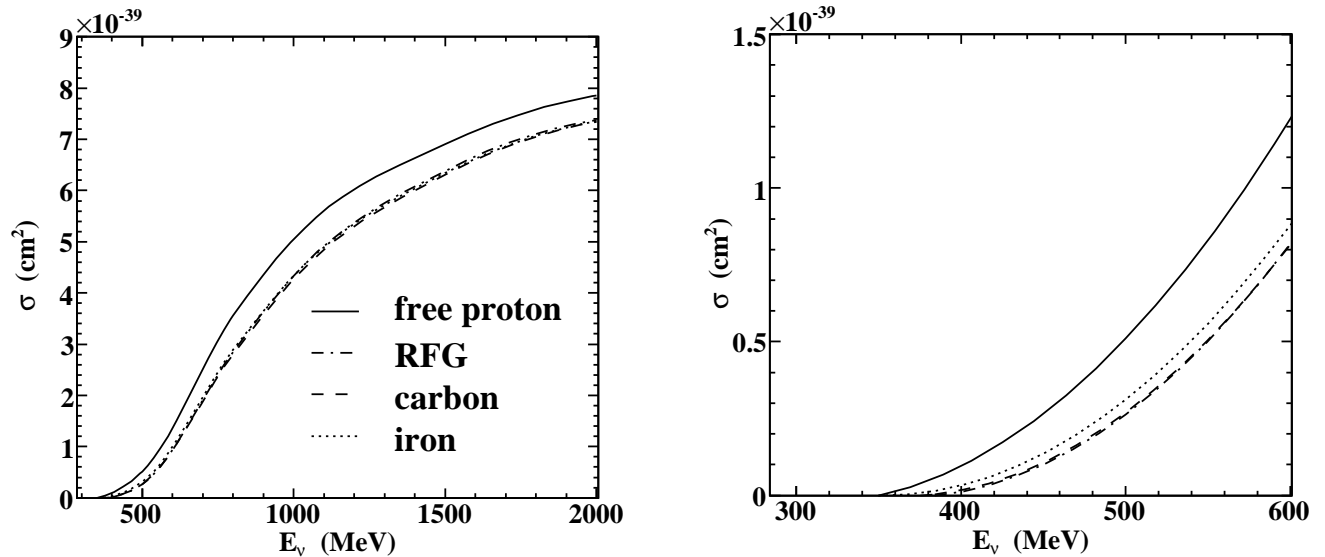
15

FIG. 6: Total cross sections per nucleon for $\nu_\mu + p \overset{\Delta^{++}}{\to} \mu^- + p + \pi^+$. The full line represents the elementary process, for scattering from a free proton. The dash-dotted line stands for the RFG calculations, whereas the dashed (dotted) line corresponds to scattering from a carbon (iron) target nucleus. The right panel focusses on the threshold region.

carbon ones. Clearly, the nuclear-target cross sections are very sensitive to binding-energy differences at lower incoming energies. These effects, however, vanish at higher neutrino energies and fall to a 1% correction level at $E_\nu = 1$ GeV. As a matter of fact, at sufficiently high energies RFG calculations with a well-chosen binding-energy correction are almost indiscernible from the corresponding RPWIA results. These findings are more detailedly assessed in Figs. 7, 8 and 9. Figures 7 and 8 compare RFG and RPWIA computations. The former considers scattering from a carbon target at $E_\nu = 800$ MeV, which corresponds to the mean energy of the neutrino beam used by the MiniBooNE experiment. As can be appreciated from Fig. 7, the RFG and RPWIA models produce almost identical results. In Fig. 8, we present the ratio of RFG to carbon RPWIA results for the twofold cross section $d^2\sigma/dT_\pi d\cos\theta_\pi^*$, where T_π is the outgoing pion's kinetic energy and θ_π^* its scattering angle relative to the neutrino-beam direction. Apart from the threshold region, where numerical instabilities induce large fluctuations, it is observed that differences between the RFG and RPWIA result do not exceed the 5% level over the whole (T_π, θ_π^*) range. In addition, the largest deviations occur where the cross section has hardly any strength. Consequently,
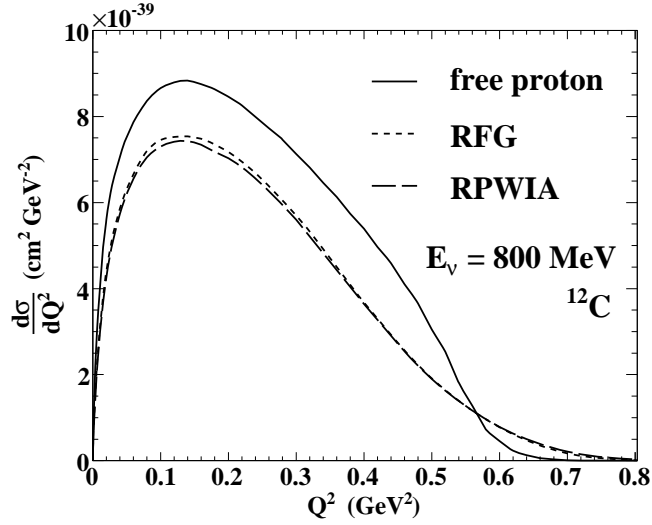
FIG. 7: Cross section per nucleon for $\nu_\mu + p \overset{\Delta^{++}}{\to} \mu^- + p + \pi^+$ on carbon at an incoming neutrino energy of 800 MeV. The full line represents the elementary process, whereas the short-dashed (long-dashed) line stands for the RFG (RPWIA) calculation.
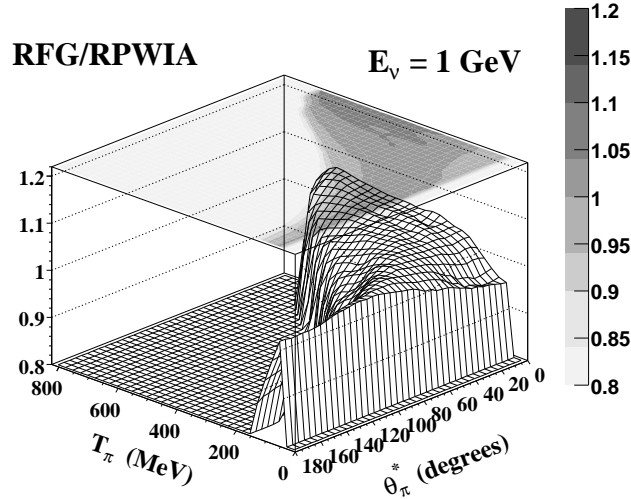

FIG. 8: Ratio of RFG to RPWIA computations for the $d^2\sigma/dT_\pi d\cos\theta_\pi^*$ cross section of the process $\nu_\mu + p \overset{\Delta^{++}}{\to} \mu^- + p + \pi^+$. A carbon target and an incoming neutrino energy of 1 GeV are considered.

upon integrating over T_π and θ_π^*, we find that the total RFG cross section exceeds the RPWIA one by about 2%. Figure 9 compares the cross section for a carbon nucleus with the one for an iron nucleus at $E_\nu = 1.5$ GeV. Although the total strength, integrated over the outgoing muon energy E_l, is the same for both nuclei, it is interesting to note that the
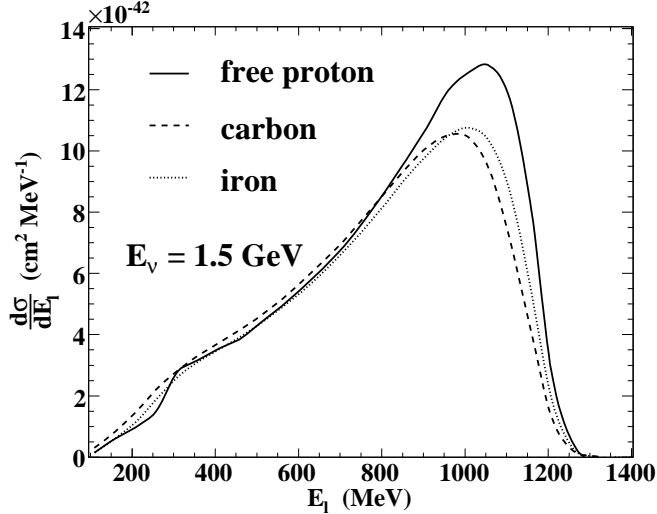
FIG. 9: The $\nu_\mu + p \overset{\Delta^{++}}{\to} \mu^- + p + \pi^+$ cross section per nucleon as a function of the lepton energy E_l for $E_\nu = 1.5$ GeV. The full line represents the elementary process, whereas the dashed (dotted) line refers to scattering from carbon (iron).

iron distribution is shifted with respect to the carbon cross section. Again, this reflects the fact that a carbon proton requires, on average, more energy than an iron proton to be knocked out of the nucleus, leaving therefore less energy for the outgoing muon. To assess the influence of medium modifications to the mass and width of the Δ, we have computed the W-distribution according to the prescription given in Eq. (38). In Fig. 10, we contrast the elementary cross section with RPWIA calculations for carbon. Compared to the free case, the RPWIA result that does not include Δ medium modifications is seen to be heavily suppressed at the Δ pole. The nuclear binding brings about a broadening of the W-distribution, mainly reallocating strength to lower invariant masses. When medium modifications are taken into account, the Δ pole is shifted towards higher W values, by an amount that corresponds to the mass shift in Eq. (38). Compared to the plain RPWIA case, the peak is again suppressed and broadened, owing to the increased medium-modified width. On the whole, we observe a 25% reduction of the RPWIA cross section when Δ medium modifications are included.
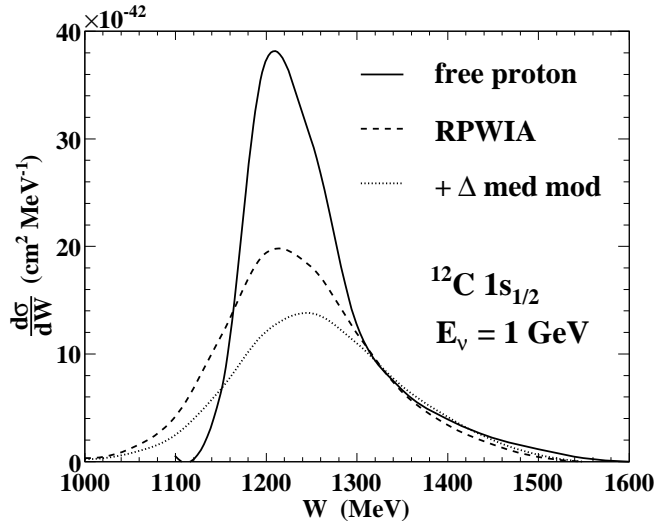
FIG. 10: Invariant-mass distribution for $\nu_\mu + p \xrightarrow{\Delta^{++}} \mu^- + p + \pi^+$ on a $1s_{1/2}$ ^{12}C proton at an incoming neutrino energy of 1 GeV. The full (dashed) line represents the calculation for a free (bound) proton. The dotted curve adds the effect of Δ medium modifications to the RPWIA result.

C. Results under MiniBooNE and K2K kinematics

In view of recent results presented by the MiniBooNE and K2K collaborations [3], we conclude this section with some computations for the specific neutrino energies and target nuclei employed by these experiments. From an experimental viewpoint, the most accessible distributions are the ones with respect to outgoing-muon variables. Fig. 11 depicts an RPWIA calculation for a two-fold differential cross section against the outgoing-muon energy and scattering angle with respect to the neutrino beam. The incoming neutrino energy is fixed at 800 MeV, corresponding to MiniBooNE's mean beam energy. Since MiniBooNE has carbon as target material, this calculation was performed on a carbon nucleus. The result shown in Fig. 11 can be integrated over θ_l or E_l to yield the one-fold cross sections displayed in Fig. 12. Relative to the free cross section, the angular distribution for a carbon target is evenly reduced by about 20%. In general, the outgoing muon prefers a forward direction, although a minor shift seems to take place between the free and the bound case. This effect relates to the change in the muon-energy distribution, depicted in the right-hand panel of Fig. 12. Indeed, for scattering off bound protons, one observes a shift of the E_l distribution towards lower values. Recognizing the correlation between high muon energies and forward
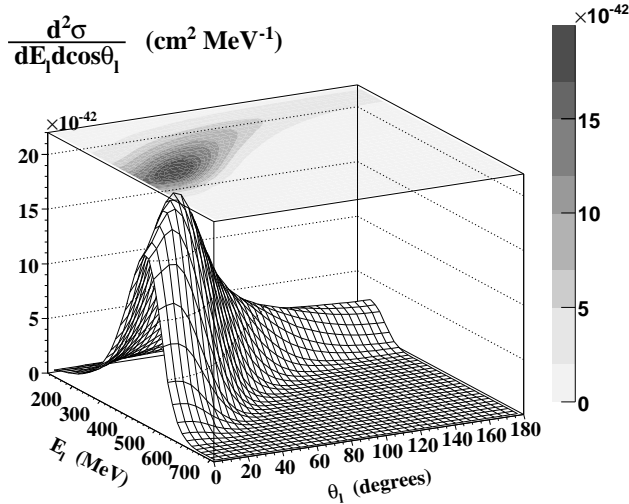
19

FIG. 11: Cross section per nucleon for $\nu_\mu + p \overset{\Delta^{++}}{\to} \mu^- + p + \pi^+$ against outgoing-muon energy and scattering angle. The incoming neutrino energy is 800 MeV, the target nucleus is carbon.

scattering angles, as can be appreciated in Fig. 11, the bound case will correspondingly yield a larger number of events at slightly higher scattering angles. We also note that the RPWIA result fades out sooner than the elementary cross section, because a certain amount of energy is needed to knock the carbon proton out of its shell. Planned experiments like MINERνA endeavor to have a good energy resolution for both the muon and the hadronic final state. The ability to detect the outgoing pion or nucleon or even both would allow a detailed study of different nuclear effects. In Figs. 13 and 14 we present cross sections versus the pion kinetic energy T_π and pion scattering angle relative to the beam direction θ_π^*. This time, we adopted K2K settings, namely an oxygen target hit by neutrinos with an energy of 1.3 GeV. From the left-hand panel of Fig. 14, one infers that, within the RPWIA model, the outgoing pion prefereably leaves the nucleus along the beam direction. As for the kinetic-energy distribution, we observe a comparable reduction and shift of the strength as in the muon-energy distribution.

V. CONCLUSION AND OUTLOOK

We have developed a relativistic framework to study Δ-mediated one-pion production from nuclei at medium energies. The proposed formalism offers great flexibility in calculating various observables both for the free process and for scattering from nuclear targets.
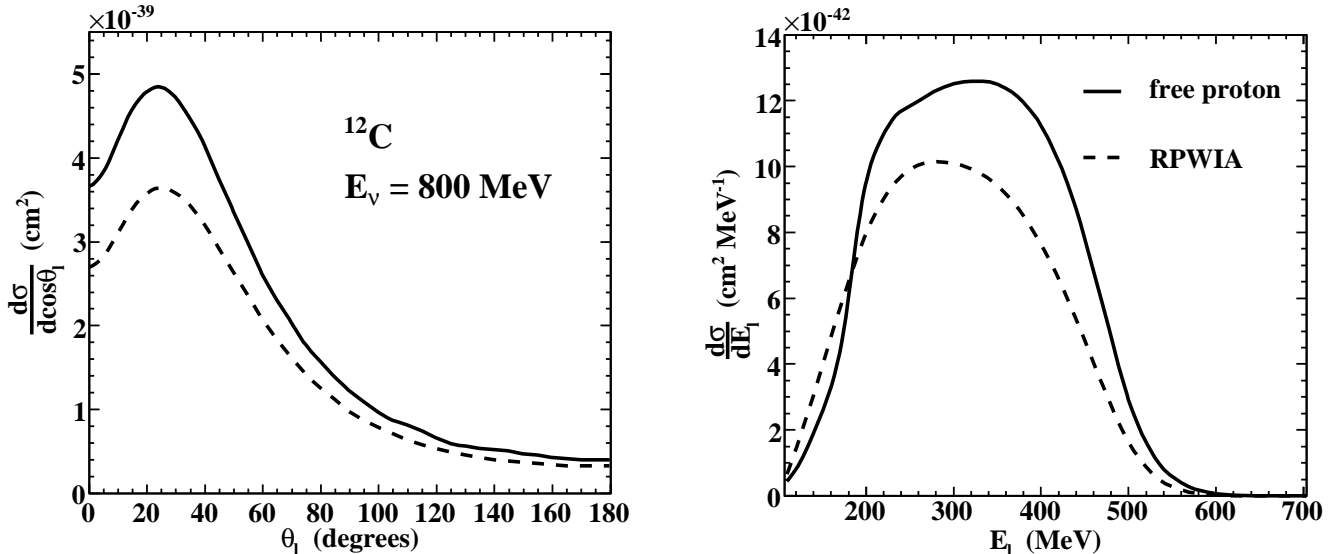
FIG. 12: Cross sections per nucleon for $\nu_\mu + p \overset{\Delta^{++}}{\to} \mu^- + p + \pi^+$, for 800 MeV neutrinos scattering from a carbon target. The left (right) panel shows the cross section as a function of the outgoing-muon scattering angle (energy). Each of the panels contrasts the elementary cross section (full line) with the RPWIA result, without Δ medium modifications (dashed line).

Motivated by operational and planned experiments, we have conducted a systematic study by addressing the impact of Δ-coupling ambiguities on the Q^2 and W distributions. Cross sections are found to vary by as much as 10% depending on whether or not the M1-dominance assumption is used to extract the vector form factors. This is very significant, as the extracted value for the axial mass M_A depends heavily on the model applied in the analysis of the neutrino-scattering data and, therefore, on a reliable input for the vector form factors. Uncertainties in the dominant axial form factor, $C_5^A(Q^2)$, have a dramatic effect on the Δ-production cross sections. At low Q^2, a 25% reduction of the off-diagonal Goldberger-Treiman value $C_5^A(0) = 1.2$ leads to cross sections that are smaller by 40%. In the case of a Q^2 dependence that is steeper than a modified-dipole form, the effect increases to almost 50% over the whole Q^2 range. In the W distribution, we observe 2%-level deviations between the traditional Δ-decay coupling choice and a consistent one, which effects a decoupling from the spin-1/2 terms. To investigate the influence of nuclear effects, we have computed RPWIA neutrino-nucleus cross sections for carbon, oxygen and iron nuclei. We have briefly touched on the topic of Δ medium modifications. Using a prescription that gives good results in
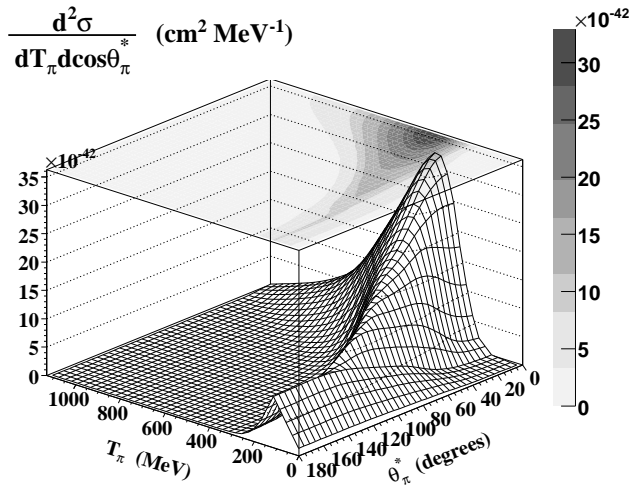
21

$$\frac{d^2\sigma}{dT_\pi dcos\theta_\pi^*} \quad (cm^2 \, MeV^{-1})$$

FIG. 13: Cross section per nucleon for $\nu_\mu + p \overset{\Delta^{++}}{\to} \mu^- + p + \pi^+$ against outgoing-pion kinetic energy and scattering angle. The incoming neutrino energy is 1.3 GeV, the target nucleus is oxygen.

photo-induced two-nucleon knockout and electron-scattering studies, we infer a 20-25% suppression of the RPWIA cross sections due to medium effects. The nuclear responses are very sensitive to binding-energy differences at lower neutrino energies. From $E_\nu = 1$ GeV onwards, the cross sections per nucleon for different nuclear targets are seen to agree at the 1% level. To assess the nuclear-model uncertainty in our description of Δ-mediated one-pion production, we have also contrasted the RPWIA results with calculations performed within an RFG model with a well-considered binding-energy correction. At 1-GeV neutrino energies, differences between one- and two-fold distributions computed within both models do not exceed the 5% level. The agreement is better for total cross sections, where deviations between the RFG and RPWIA model dwindle to 1-2%. Hence, for sufficiently high incoming neutrino energies, the influence of Fermi motion, nuclear binding and the Paul exclusion principle can be well described by adopting an RFG model with binding-energy correction. The RFG model, however, just as the RPWIA approach, falls short in implementing FSI and nuclear correlations of the short and long-range type. Contrary to the RFG, the model proposed in this work has the important advantage that it can serve as a starting point for a relativistic and quantum-mechanical study of FSI mechanisms. As a matter of fact, the inclusion of FSI for the ejected pions and nucleons is currently under study. To this end, we closely follow the lines of Ref. [33], where use is made of a relativistic Glauber model for
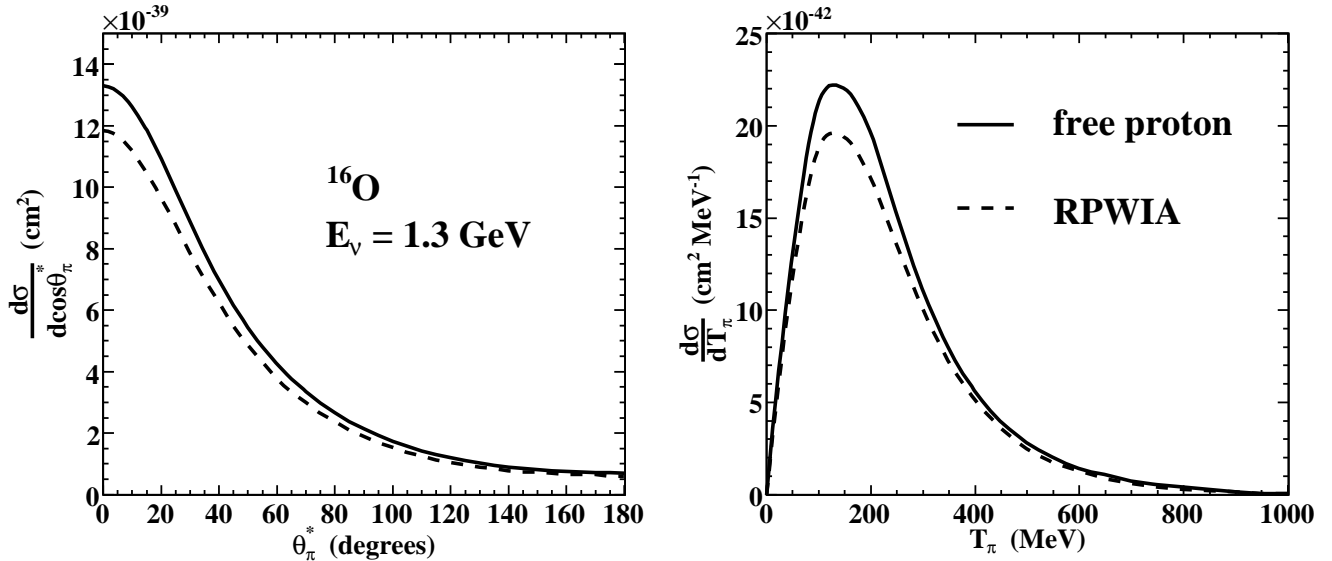
FIG. 14: Cross sections per nucleon for $\nu_\mu + p \overset{\Delta^{++}}{\to} \mu^- + p + \pi^+$, for 1.3 GeV neutrinos scattering from an oxygen target. The left (right) panel shows the cross section as a function of the outgoing-pion scattering angle (kinetic energy). Each of the panels contrasts the elementary cross section (full line) with the RPWIA result, without Δ medium modifications (dashed line).

fast ejectiles and an optical-potential approach for lower ejectile energies.

Acknowledgments

[1] BooNE Collaboration home page http://www-boone.fnal.gov/.

[2] K2K Collaboration home page http://neutrino.kek.jp/.

[3] R. Tayloe (MiniBooNE collaboration), in *Proceedings of NuInt07: the 5th international workshop on neutrino-nucleus interactions in the few-GeV region, Batavia, 2007*, edited by G. P. Zeller, J. G. Morfin and F. Cavanna (Melville, New York, 2007), p. 39; L. Whitehead and A. Rodriguez (K2K collaboration), *ibid.* p. 169.

[4] S. Boyd (MINERνA), Nucl. Phys. Proc. Suppl. **139**, 311 (2005).

[5] SciBooNE Collaboration home page http://www-sciboone.fnal.gov/.

[6] D. Rein and L. M. Sehgal, Ann. Phys. (N.Y.) **133**, 79 (1981).

[7] K. M. Graczyk and J. T. Sobczyk, Phys. Rev. D **77**, 053001 (2008).

[8] O. Lalakulich and E. A. Paschos, Phys. Rev. D **71**, 074003 (2005).

[9] O. Lalakulich, E. A. Paschos and G. Piranishvili, Phys. Rev. D **74**, 014009 (2006).

[10] E. Hernández, J. Nieves and M. Valverde, Phys. Rev. D **76**, 033005 (2007).

[11] K. S. Kuzmin, V. V. Lyubushkin and V. A. Naumov, Acta Phys. Pol. B **37**, 2337 (2006).

[12] D. Barquilla-Cano, A. J. Buchmann and E. Hernández, Phys. Rev. C **75**, 065203 (2007).

[13] C. Alexandrou, Th. Leontiou, J. W. Negele and A. Tsapalis, Phys. Rev. Lett. **98**, 052003 (2007).

[14] C. Alexandrou, G. Koutsou, Th. Leontiou, J. W. Negele and A. Tsapalis, Phys. Rev. D **76**, 094511 (2007).

[15] V. Pascalutsa and R. Timmermans, Phys. Rev. C **60**, 042201 (1999).

[16] C. J. Horowitz, H. Kim, D. P. Murdock and S. Pollock, Phys. Rev. C **48**, 3078 (1993).

[17] W. M. Alberico, M. B. Barbaro, S. M. Bilenky, J. A. Caballero, C. Giunti, C. Maieron, E. Moya de Guerra and J. M. Udías, Nucl. Phys. **A623**, 471 (1997).

[18] M. C. Martínez, P. Lava, N. Jachowicz, J. Ryckebusch, K. Vantournhout and J. M. Udías, Phys. Rev. C **73**, 024607 (2006).

[19] O. Benhar, A. Fabrocini, S. Fantoni and I. Sick, Nucl. Phys. **A579**, 493 (1994).

[20] O. Benhar, N. Farina, H. Nakamura, M. Sakuda and R. Seki, Phys. Rev. D **72**, 053005 (2005).

[21] O. Benhar and D. Meloni, Nucl. Phys. **A789**, 379 (2007).

[22] A. M. Ankowski and J. T. Sobczyk, arXiv:0711.2031 [nucl-th].

[23] E. Oset and L. L. Salcedo, Nucl. Phys. **A468**, 631 (1987).

[24] T. Leitner, L. Alvarez-Ruso and U. Mosel, Phys. Rev. C **73**, 065502 (2006).

[25] S. Ahmad, M. S. Athar and S. K. Singh, Phys. Rev. D **74**, 073008 (2006).

[26] R. J. Furnstahl, B. D. Serot and H.-B. Tang, Nucl. Phys. **A615**, 441 (1997).

[27] P. Lava, N. Jachowicz, M. C. Martínez and J. Ryckebusch, Phys. Rev. C **73**, 064605 (2006).

[28] C. Praet, N. Jachowicz, J. Ryckebusch, P. Vancraeyveld and K. Vantournhout, Phys. Rev. C **74**, 065501 (2006).

[29] N. Jachowicz, P. Vancraeyveld, P. Lava, C. Praet and J. Ryckebusch, Phys. Rev. C **76**, 055501 (2007).

[30] J. Bjorken and S. Drell, Relativistic Quantum Mechanics, (McGraw-Hill, N.Y. 1964).

[31] P. Stoler, Phys. Rept. **226**, 103 (1993).

[32] E. A. Paschos, J.-Y. Yu and M. Sakuda, Phys. Rev. D **69**, 014013 (2004).

[33] W. Cosyn, M. C. Martínez and J. Ryckebusch, Phys. Rev. C **77**, 034602 (2008).

[34] S. Gardner and J. Piekarewicz, Phys. Rev. C **50**, 2822 (1994).

[35] I. J. D. MacGregor et al., Phys. Rev. Lett. **80**, 245 (1998).

[36] K. L. G. Heyde, *The Nuclear Shell Model* (Springer-Verlag, Berlin, 1994).